electrochem

MDPI

Article

Copper-Doped Tin Oxide for Enhancing the Electrochemical Conversion of CO_2 to Formate

Pom Lal Kharel [1,*], Muthu Kumaran Gnanamani [2], Md Ariful Hoque [2], Keemia Abad [1,3], Ayokunle O. Omosebi [1] and Jesse Thompson [1,3,*]

[1] Institute for Decarbonization and Energy Advancement, University of Kentucky, Lexington, KY 40506, USA; keemia.abad@uky.edu (K.A.)
[2] Center for Applied Energy Research, University of Kentucky, Lexington, KY 40511, USA; muthu.gnanamani@uky.edu (M.K.G.)
[3] Department of Chemistry, University of Kentucky, Lexington, KY 40506, USA
* Correspondence: pkharel.6169@gmail.com (P.L.K.); jesse.thompson@uky.edu (J.T.)

Abstract

Bimetallic electrocatalysts show great promise in enhancing catalytic activity and selectivity compared to their monometallic counterparts by enabling precise tuning of structure, morphology, and composition. Sn-based bimetallic electrocatalysts have emerged as promising materials for the electrochemical conversion of CO_2 to formate/formic acid. The interaction between tin and a second metal can facilitate electron transfer, regulate adsorption strength of reaction intermediates (HCOO*), and enhance catalytic activity and product selectivity. This study employs a copper-doped tin oxide catalyst with 95 mol% Sn and 5 mol% Cu immobilized on carbon xerogel for the electrochemical CO_2 reduction to formate in a flow cell setup. This led to an impressive maximum Faradaic efficiency of 94% at a cell potential of 3.8 V, maintaining a notable Faradaic efficiency over 80% even after 200 h of continuous operation. The production of formate was also consistent with the FE observed. A high-level techno-economic analysis was conducted to assess the viability of the electrocatalyst system to assess the conversion of CO_2 based on the experimental data. The techno-economic analysis reveals that the production price of formic acid is very similar to the current commercial price making the proposed system for converting CO_2 into a commercial product. This system coupled with post-combustion carbon system not only reduces the CO_2 concentration in the flue gas, but also produces high-energy-value chemicals at the same time.

Keywords: electrochemical; techno-economic; flow cell; bimetallic; copper-doped; bipolar

Check for updates

Academic Editor: Bastian Mei

Received: 4 October 2026
Revised: 24 November 2026
Accepted: 24 November 2026
Published: 26 November 2026

Copyright: © 2026 by the authors. Licensee MDPI, Basel, Switzerland. This article is an open access article distributed under the terms and conditions of the Creative Commons Attribution (CC BY) license.

1. Introduction

The electrochemical reduction of CO_2 to formate/formic acid (FA) is at the forefront of electrochemical carbon utilization technology. The advantages include: (i) the reaction is favored thermodynamically, (ii) the reduction product formate/FA is easier to handle and store compared to a gaseous product, and (iii) given that the potential production cost of FA could be cheaper, and could provide an additional life-cycle reduction in CO_2 emission, compared to the Kemira process, there are potential markets for FA, such as direct formic acid fuel cells and as an effective medium for liquid H_2 storage [1–4]. The metallic electrocatalysts including Pb, Hg, In, Sn, Bi, Cd, and Ti are the most investigated catalysts for the electrochemical conversion of CO_2 to formate/FA. Recent reports reveal that metal-free electrocatalysts are also effective in reducing CO_2 to formic acid and other products [5–7].

Numerous electrocatalysts including Bi and Bi oxides, Cu-based composites, Sn and Sn-based electrocatalysts, and nano In/Ag composites are studied for the electrochemical conversion of CO_2 to formate/FA [8–19]. Metallic Sn is considered the catalytically active phase for the electrochemical reduction of CO_2 to FA, owing to its superior thermodynamic stability under electrolytic CO_2 reduction conditions [20,21]. Sn-coated metal plates have been employed as electrodes for the electrochemical reduction of CO_2 to formate. However, their relatively limited interfacial surface area restricts the availability of dissolved CO_2 near the catalyst surface, thereby posing challenges for efficient operation at high current densities [22,23]. The chemical transformation of Sn during the electrochemical process is additional issue with the use of Sn. More recent approaches have used nanoparticle-based catalysts made of Sn mainly in the form of SnO_2 [24–26]. Additionally, Sn and Sn-based catalysts are well focused materials due to the superiorities of their nontoxicity, earth abundance, and low cost [27–29]. Tin sulfide (SnS or SnS_2) is attracting a lot of interest because of its simplicity in synthesis and selectivity [30]. Furthermore, modified tin sulfides have been reported as electrocatalysts with good selectivity for formate/FA [31]. Metal-doping has been an interest to control the electronic properties of SnO_2 nanoparticles. Atomic level doping of Co, Cu, Bi, or Pt into tin oxide has been shown to improve the selectivity and stability for FA production [32–34]. However, many of these investigations have been limited in duration, with catalyst performance showing signs of decline over time. Although Cu and Cu-based catalysts are associated with hydrocarbon selectivity, recent studies reveal that nano Cu and Cu oxides are capable of reducing CO_2 to formate/FA with exceptionally high selectivity, but at extremely pressurized conditions [35–37]. Reports reveal that synergistic bimetallic electrocatalysts can improve the activity and selectivity compared to their monometallic counterparts by fine-tuning their structure, morphology, and composition [38–42]. Various Sn-based bimetallic electrocatalysts have demonstrated to promote the electrochemical conversion of CO_2 to formate/FA [43–48]. Recent reports on bimetallic Sn-Cu electrocatalyst showed significant progress to enhance the selectivity and efficiency of formate/FA production [49–51]. The electrochemical reduction of CO_2 gas to formate/FA requires attention to address several significant challenges that limit its large-scale industrial application. One major issue is the narrow potential window required for formate/FA production, meaning the reaction only occurs efficiently within a very limited voltage range. In addition, the process often suffers from high overpotential, which increases energy consumption and reduces overall efficiency. Long-term operational stability is another concern because electrolytes can precipitate over time, and catalysts may undergo structural or chemical transformations that decrease their activity and durability. Furthermore, the synthesis of effective catalysts is frequently complex, time-consuming, and expensive, making commercial implementation difficult. Despite these limitations, the studies discussed do not provide high-level techno-economic analyses based on data obtained from the electrochemical reduction of CO_2 gas, helping researchers evaluate the feasibility, cost, and future potential of this technology for sustainable fuel and chemical production.

Our previous studies have demonstrated the significant capabilities of copper-doped tin oxide immobilized on carbon xerogel as an efficient electrocatalyst for the conversion of CO_2 gas into formate with high selectivity. These investigations highlighted that the catalyst maintained strong performance even when tested in an H-cell configuration, a system typically limited by substantial mass transfer constraints and increased ohmic resistance [52,53]. This electrochemical system was effective to mitigate the mass transfer limitations caused by poor solubility of CO_2 and the minimization of salt precipitation on the surface of gas diffusion electrode (GDE) through the coupling of a suitable bicarbonate solution with CO_2 gas, thereby maintaining electrode stability and sustained catalytic activity over extended operation.

In this study, the bimetallic SnCu oxide catalyst containing 95 mol% of Sn and 5 mol% of Cu was employed for electrochemical CO_2 reduction in a flow cell configuration using an aqueous KOH solution as a catholyte, pure CO_2 gas as a source and aqueous H_2SO_4 solution as an anolyte. Remarkably, the maximum FE of 94% was achieved for formate at the cell potential 3.8 V. Our electrochemical system consistently was found to generate formate at a steady rate of 24 mmol/day over a continuous operation period of 200 h. The production of formate was also consistent with the FE observed. The electrochemical data strongly supports the observed results of formate production at 3.8 V. Additionally, this study presents a high-level techno-economic analysis (TEA) to assess the viability of the electrocatalyst system to reduce greenhouse gas (GHG) emissions from point sources based on the experimental data.

2. Experiments and Methods

2.1. Chemicals and Materials

Flow cell with 5 cm^2 area that mimics the commercial electrochemical reactor was purchased from Dioxide Materials (Boca Raton, FL, USA). Fumasep FBM (bipolar membrane), nafion dispersion (5% in isopropanol), and commercial plain carbon cloth, were purchased from FuelCellStore (Bryan, TX, USA). Potassium carbonate (ACS reagent, ≥99.0%), potassium bicarbonate (ACS reagent, ≥99.7%), sulfuric acid (ACS reagent, 95.0–98.0%), sodium carbonate (ACS reagent, ≥99.5%), resorcinol (ACS reagent grade, ≥99.0%), ethanol (anhydrous, ≥99.5%), isopropanol (anhydrous, ≥99.5%), and acetone (ACS reagent, ≥99.5%) were purchased from Sigma Aldrich (St. Louis, MO, USA).

2.2. Synthesis of Catalyst

The bimetallic $Sn_{95}Cu_5$ oxide catalyst was synthesized according to our previously published procedure [52]. Copper nitrate ($Cu(NO_3)_2{\cdot}3H_2O$) and tin chloride ($SnCl_2{\cdot}2H_2O$) served as the copper and tin precursors, respectively. For a typical synthesis, 4.29 g of tin chloride (19 mmol) was dissolved in 150 mL of deionized water and stirred at 5–10 °C using an ice bath. Separately, 0.24 g of copper nitrate (1 mmol) was dissolved in 50 mL of deionized water at the same temperature. The copper solution was then combined with the tin solution under vigorous stirring conditions, maintaining the temperature, and was stirred for an additional hour. Subsequently, 5.6 mL of ammonium hydroxide (28.3%) was added dropwise. The resulting precipitate was filtered, washed with deionized water followed with anhydrous ethanol, and dried under vacuum at room temperature for 24 h. From this material, 1 g of the dried sample was dispersed in 100 mL of a 70:30 ethanol-water (*v:v*) mixture within a round-bottom flask and refluxed overnight at 80 °C. The final product was filtered, washed thoroughly with anhydrous ethanol, and dried.

2.3. Synthesis of Carbon Xerogel

Mesoporous carbon xerogel (CX) was synthesized on commercial carbon via resorcinol–formaldehyde polymerization catalyzed by sodium carbonate, following a reported method [52,54]. Adequate amounts of resorcinol, formaldehyde, deionized water, and sodium carbonate were mixed together and stirred to form a clear solution, which was spread onto carbon cloth and sandwiched between glass plates. The assembly was heated at 100 °C for 30 h, then the cloth was washed with water and acetone for 2h each. Finally, it was heat-treated and cooled on its own in nitrogen.

2.4. Catalyst Coating

Airbrushing method was used to make the working electrodes in this study. First ink solution was prepared by sonicating a mixture of catalyst, activated carbon, alcohol-based

nafion dispersion, deionized water, and isopropanol, and it was then spray-coated on the mesoporous carbon xerogel supported on commercial carbon cloth with catalyst loading of 2.42 mg cm^{-2}. This is referred to as the catalyst-coated electrode (CCE), serving as a cathode. Similarly, PtIr was coated on the carbon xerogel by airbrushing the ink solution where the catalyst PtIr nanoparticles were well dispersed in isopropanol and nafion dispersion. This is the counter electrode, serving as an anode where oxidation of water to O_2 takes place. The catalyst loading for the counter electrode was 2.56 mg cm^{-2}.

2.5. Flow Cell Design

The configuration of the flow cell reported here is depicted in Figure 1. The compact flow cell consisted of GDEs (cathode and anode) and Fumasep bipolar membrane (BPM) sandwiched between Ti-plate, the anode endplate and Ni-plate, the cathode end plate. The system was made leak-free with Si and PTFE gaskets. The middle flow channel helps to regulate a smooth flow of catholyte into and out of the cathode chamber.

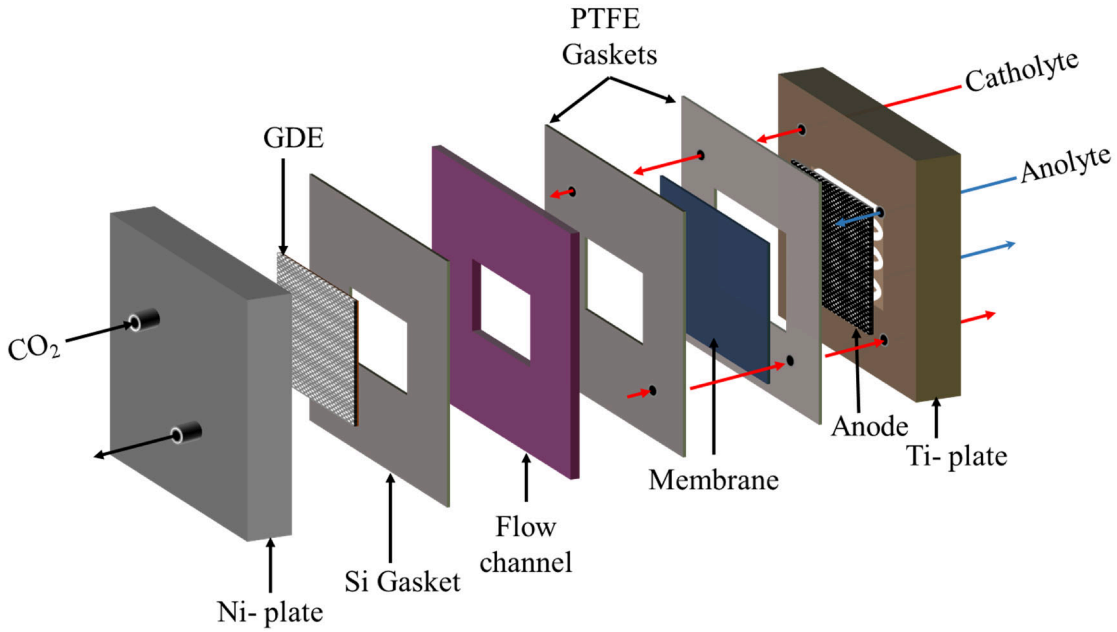

Figure 1. Configuration of flow cell where GDEs serving as cathode and anode are sandwiched between Ti-plate (anode endplate) and Ni-plate (cathode endplate). The cathodic and anodic chambers are separated from each other by a membrane.

The GDE and the operational scheme of the electrochemical process are shown in Figure 2a,b. Basically, there three regions labeled as ❶, ❷ and ❸ in Figure 2b. The BPM after getting a sufficient voltage from the source causes dissociation of water into H^+ and OH^- ions: $H_2O \rightarrow H^+ + OH^-$ (region ❷). These ions then diffuse towards the chambers having oppositely charged electrodes. The GDE serves as a medium for the diffusion of gases from one chamber to another, and the catalyst catalyzes. The GDE at the cathode facilitates the diffusion of CO_2 gas to the catalyst layer where it meets the catholyte and the protons from BPM and gets reduced to formate as $CO_2 + H^+ + 2e^- \rightarrow HCOO^-$ (region ❶). Similarly, O_2 gas is produced at anode due to oxidation of OH^- ions as $4OH^- \rightarrow 2H_2O + O_2 + 4e^-$ (region ❸). The GDE at anode helps O_2 exit from the cell. Catholyte and anolyte are pumped into the cell at the flow rate of 2 mL/min and 10 mL/min, respectively, using peristaltic pumps. These flow rates were adjusted to maintain the same pressure drop across the anodic and cathodic chambers.

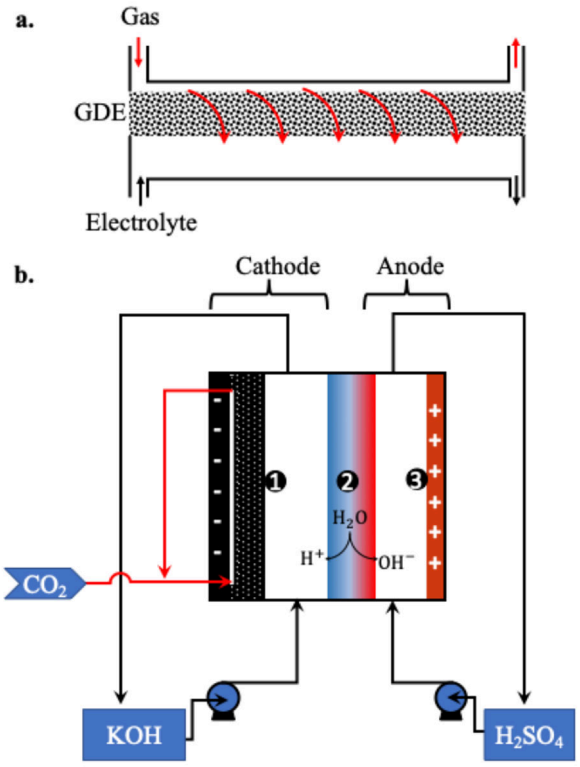

Figure 2. (**a**) A gas diffusion electrode, and (**b**) scheme for the operation of flow cell.

Electrochemical measurements were conducted employing 0.4 M KOH (aq) as the catholyte and 0.4 M H_2SO_4 (aq) as the anolyte, with a Fumasep BPM serving as a separator. The reverse bias mode with the BPM facilitates water-splitting, generating protons that diffuse to the cathodic chamber through its cation exchange layer and hydroxide ions to the anodic chamber through the anion exchange layer. While alkaline solutions are typically utilized as anolytes with bicarbonate catholyte solutions to mitigate potential losses stemming from pH variations, studies have revealed that in an alkaline environment, the anion exchange layer of the BPM deteriorates over time, leading to increased resistance towards water-splitting [55]. Although employing an acid as an anolyte with a BPM may lead to some potential losses and could necessitate the use of a precious metal for the anode, the stability of the BPM's anion exchange layer benefits from contact with acid. Our electrochemical flow cell uses the CX with $Sn_{95}Cu_5$ catalyst (CX_$Sn_{95}Cu_5$) as the cathode and PtIr catalyst (CX_PtIr) as the anode.

Prior to any electrochemical measurement, dry N_2 gas was purged into the catholyte solution for 15 min to remove dissolved O_2. Subsequently, water-saturated CO_2 gas was introduced into the cell at a rate 10 mL/min. Chronoamperometric measurements were then performed at various cell potentials to identify the optimum performance of the electrochemical cell. Following this optimization, the cell's stability and formate production were determined at the optimal cell potential. The total charge (Q_T) used for assessing the catalytic performance was calculated by integrating current (i) with respect to time (t) as:

$$Q_T = \int_0^t i dt.$$

Liquid samples were extracted from the catholyte reservoir at different time intervals during the experimental run for formate analysis.

2.6. Quantification of Formate

Formate production was quantified using a Dionex ICS-6000 Ion Chromatography (IC) system (Dionex-Thermo Scientific, Sunnyvale, CA, USA) equipped with an AS autosampler. The anion analysis setup included an ADRS 600 suppressor, an EGC 500 KOH eluent generator, an IonPac AS15 analytical column, and an AG15 guard column. Isocratic elution was carried out using 15 mM KOH as the mobile phase over a 12 min run.

A certified formate standard solution (100 mg/L) was purchased from Environmental Express (Charleston, SC, USA). Calibration standards of different concentrations were prepared through serial dilution of the stock solution using 18.2 MΩ ultrapure water. Before IC analysis, the collected samples were appropriately diluted, and each sample was analyzed in triplicate to ensure reproducibility. Chromatographic peaks were manually identified and integrated using Dionex Chromeleon chromatography management software (version 7). The formate concentration in the liquid phase ($C_{formate}$) was determined from a calibration curve generated using the standard formate solutions. The resulting calibration relationship was subsequently used to calculate the total number of moles of formate produced ($N_{formate}$) as follows:

$$N_{formate} = C_{formate}\ (M) \times V_{ele}\ (L)$$

where V_{ele} is the volume of the electrolyte used during the electrochemical measurement (500 mL in our case).

The performance of the flow cell for the electrochemical reduction of CO_2 to formate was evaluated with respect to the Faradaic efficiency (FE) and amount of formate produced. The FE was calculated as:

$$FE = \frac{2 \times 96485\ \left(\frac{C}{mol}\right) \times N_{formate}\ (mol)}{Q_T} \times 100\%$$

where $N_{formate}$ is the number of moles of formate produced when a total charge of Q_T is passed through the cell, calculated using above equation. Furthermore, the rate of formate production $rate_{formate}$ was derived from $N_{formate}$, normalized by time (t) as:

$$rate_{formate} = \frac{N_{formate}}{t}$$

3. Results and Discussion

Mesoporous CX has emerged as an excellent substrate for the fabrication of catalyst-coated GDEs owing to its high electrical conductivity, large surface area, and strong ability to anchor catalyst particles [52]. These properties make CX particularly suitable for electrochemical applications where efficient charge transport and catalyst stability are critical. The porous network of CX facilitates uniform catalyst dispersion while also enhancing mass transport, thereby contributing to improved electrode performance. Scanning electron microscopy (SEM) images presented in Figure 3a,b reveal the surface morphology of the prepared GDEs. The images clearly demonstrate that catalyst particles are firmly adhered to the mesoporous CX substrate. For the CX_$Sn_{95}Cu_5$ electrode (Figure 3a), the catalyst particles are uniformly distributed across the CX surface without noticeable agglomeration. Similarly, the CX_PtIr electrode (Figure 3b) exhibits a homogeneous dispersion of PtIr catalyst particles, indicating effective interaction between the catalyst and the CX support. Such uniform distribution is essential for maximizing the electrochemically active surface area and ensuring consistent catalytic activity throughout the electrode. To further confirm the chemical composition of the catalysts, energy-dispersive X-ray spectroscopy (EDS) analysis was performed on both the as-synthesized $Sn_{95}Cu_5$ oxide and the commercial PtIr catalyst.

The EDS spectra shown in Figure 3c–e confirm the presence of the expected elements. In the SnCu oxide catalyst, the molar ratio of Sn to Cu closely matches the targeted stoichiometric composition of 95:5, indicating successful synthesis and compositional control. The XRD spectra of the catalyst reported in our previous work reveals that Cu was doped into Sn oxide, showing the peaks related to SnCu oxides and changing some of the lattice parameters [52]. Likewise, the PtIr catalyst displays approximately equimolar proportions of Pt and Ir, consistent with its commercial specification. The catalyst particles are well dispersed with 2.42 mg cm^{-2} loading of $Sn_{95}Cu_5$ oxide on the cathode and 2.56 mg cm^{-2} of PtIr on the anode.

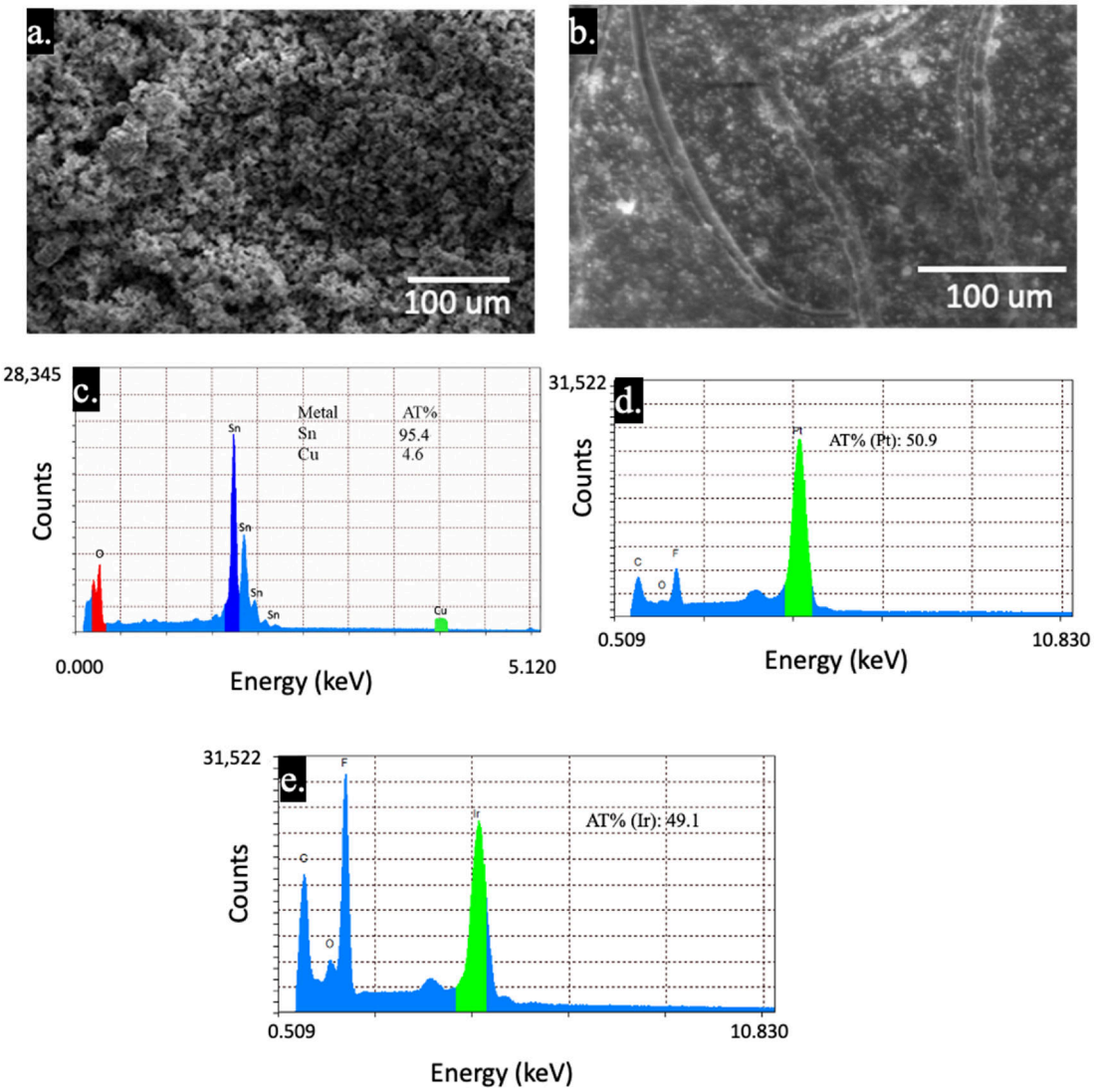

Figure 3. (**a**) The SEM image of CX coated with $Sn_{95}Cu_5$ oxide (CX_$Sn_{95}Cu_5$) serving as a cathode, (**b**) the SEM image of CX coated with PtIr (CX_PtIr) serving as an anode, (**c**) the EDS spectra of as prepared $Sn_{95}Cu_5$, and (**d**,**e**) the EDS spectra of commercial PtIr.

The electrochemical performance of the system was evaluated using a flow cell configured as shown in Figure 1. The cathodic compartment was supplied with 0.4 M KOH as the catholyte, while 0.4 M H_2SO_4 was used as the anolyte. This configuration was selected to ensure efficient ionic conductivity and stable operation under alkaline cathodic and acidic anodic conditions. The cell was operated at a range of applied cell potentials from 3.4 V to 4.4 V to investigate the effect of operating voltage on current response and product selectivity during CO_2 electroreduction.

At each applied cell potential, the system was operated continuously for a duration of 2–3 h using a fresh catholyte and the total current passing through the cell was recorded as a function of time. The total current refers to the sum of currents arising due to the electrochemical oxidation and reduction in the process. This approach allowed for the assessment of both electrochemical stability and steady-state performance under each operating condition. The FEs for formate production were calculated based on the quantified liquid products and the total charge passed, and the corresponding current densities (CDs) were determined using the geometric electrode area of 5 cm^2. Figure 4a summarizes the relationship between applied cell potential, FE for formate, and CD. At cell potentials below 3.4 V, the FE for formate production remained below 10%, indicating insufficient driving force for effective CO_2 reduction under these conditions. Similarly, at higher cell potentials exceeding 4.3 V, the FE for formate again decreased to below 10%, suggesting that competing side reactions, such as hydrogen evolution, became dominant at elevated voltages. A significant increase in both FE and current density was observed once the cell potential exceeded 3.5 V. This sharp rise indicates the onset of kinetically favorable CO_2 reduction to formate. The FE for formate reached a maximum value of 94% at an applied cell potential of 3.8 V, demonstrating excellent selectivity toward formate formation under these conditions. At this optimal potential, the total current density attained a value of -22.9 mA cm^{-2}, reflecting efficient electron utilization for the desired reaction pathway. The variation in formate production is consistent with the trend observed for formate FE, indicating that below and above the optimized cell potential parasitic reactions are dominant. Under the experimental conditions of our electrochemical setup, the rate of formate formation was therefore strongly dependent on the applied cell potential, reaching its maximum at the same potential where the FE was highest. This correlation underscores the importance of optimizing the operating voltage to balance reaction kinetics and selectivity. As illustrated in Figure 4b, significant formate production was sustained within a cell potential window ranging from 3.7 V to 4.0 V, and was at its maximum at 47.8 mmol/day. Outside this range, selectivity toward formate diminished markedly. These results highlight the critical role of applied cell potential in governing both the efficiency and productivity of CO_2 electroreduction in the flow cell system.

The liquid-phase products formed during CO_2 electroreduction were carefully sampled and analyzed to identify any reduced carbon species. The analysis revealed that no additional C_1 or C_2 liquid products were detected apart from formate, indicating high selectivity of the reaction pathway under the investigated conditions. Complementary gas chromatographic analysis of the gaseous products showed that hydrogen was the only detectable gaseous byproduct. These observations suggest that the cathodic reactions were limited to formate formation from CO_2 reduction and hydrogen evolution via the hydrogen evolution reaction (HER). Based on the assumption that only formate and hydrogen were produced at the cathode, the partial CDs corresponding to formate production and hydrogen evolution were calculated and are presented in Figure 5a. A notable dependence of product distribution on the applied cell potential was observed. In the potential range between 3.7 and 4.0 V, the partial CD for hydrogen evolution was significantly suppressed, while the partial CD for formate formation increased. This behavior clearly indicates that the catalyst selectively favors CO_2 reduction to formate over HER within this potential window. The suppression of HER is particularly important, as hydrogen evolution is a major competing reaction that often limits the efficiency of desired CO_2 electroreduction processes.

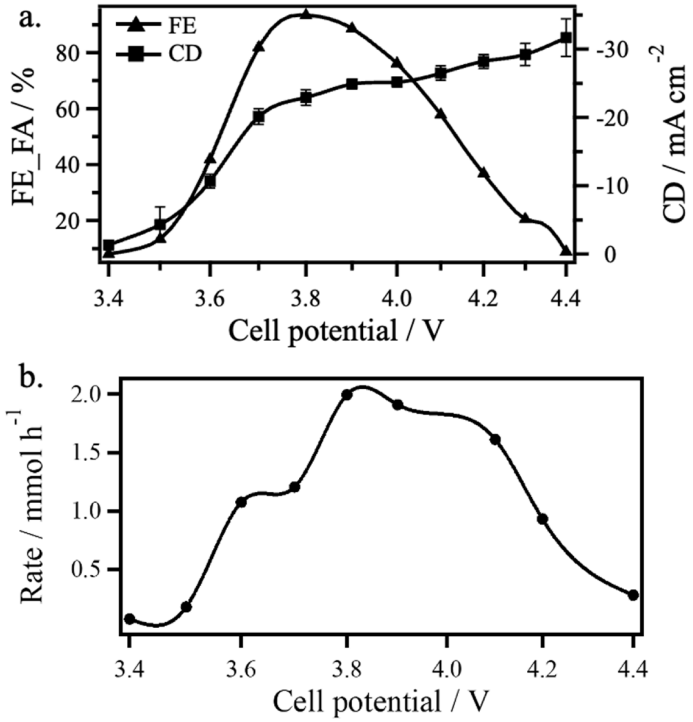

Figure 4. (**a**) The FEs for formate and CDs observed at different cell potentials on the GDE CX_$Sn_{95}Cu_5$. Maximum FE of 94% with a CD of −22.9 mA cm^{-2} was observed at 3.8 V. The error bars in CDs represent the standard deviation of CD during measurement time. (**b**) Rate of formate production with cell potential.

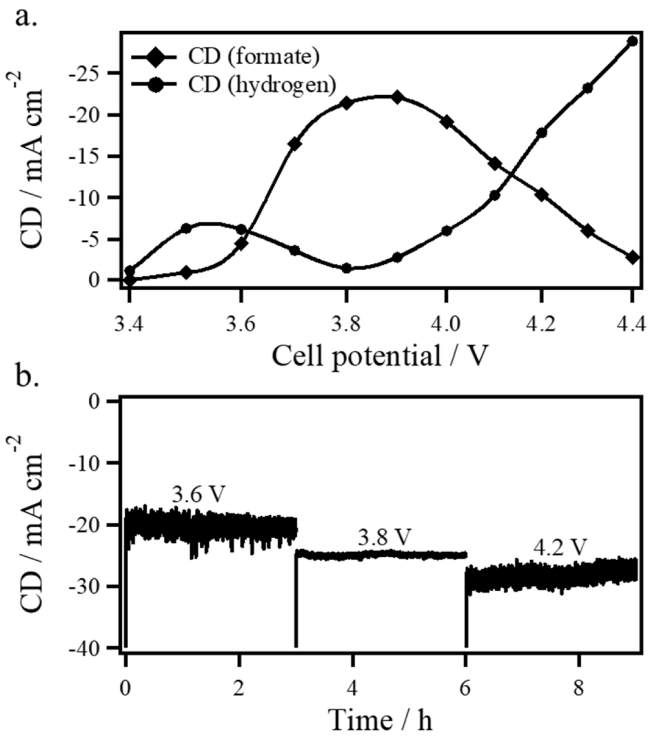

Figure 5. (**a**) Variation of partial CDs for formate and hydrogen as a function of cell potential. The partial CD for H_2 is significantly suppressed in the region 3.7 to 4.0 V while that of formate is increased, indicating that our catalyst is suppressing HER for formate. (**b**) The chronoamperometric plots at 3.6 V, 3.8 V and 4.2 V, showing HER above and below 3.8 V.

At cell potentials exceeding 4.0 V, the partial CD associated with hydrogen evolution increased sharply, becoming the dominant reaction. This shift suggests that at higher cell potentials, the thermodynamic and kinetic favorability of HER outweighs that of CO_2 reduction, thereby reducing formate selectivity. Such behavior is commonly observed in electrochemical CO_2 reduction systems and highlights the importance of optimizing operating potentials to achieve selective product formation. The partial CD profiles also exhibited larger fluctuations at cell potentials of 3.6 V and 4.2 V compared to those observed at 3.8 V. These fluctuations are attributed to the formation and accumulation of hydrogen gas bubbles on the cathode surface, which is exacerbated by the relatively slow flow rate of the catholyte. Gas bubble formation can temporarily block active sites and hinder mass transport, leading to instability in the measured current densities. In contrast, the smoother current response at 3.8 V suggests more stable reaction conditions and more efficient gas removal or no gas bubble formation. Further evidence for HER suppression was obtained from chronoamperometric measurements conducted at cell potentials of 3.6 V, 3.8 V, and 4.2 V, as shown in Figure 5b. The average CDs recorded over a three-hour period were -20.1 ± 1.16 mA cm^{-2} at 3.6 V, -24.9 ± 0.34 mA cm^{-2} at 3.8 V, and -28.2 ± 1.00 mA cm^{-2} at 4.2 V. The uncertainty in each CD represents the one standard deviation of fluctuation during the time of measurement. This arises when there is bubble formation. When the size of the bubble keeps increasing, the CD keeps decreasing because of the resistance created by the bubble. As soon as the bubble bursts, the CD increases sharply. The relatively low standard deviation at 3.8 V indicates superior operational stability compared to the other potentials in suppressing HER. Above and below 3.8 V, the noise level is found to be increasing. Overall, these results confirm that the catalyst effectively suppresses hydrogen evolution and promotes selective formate production within an optimal potential range, demonstrating its promise for efficient CO_2 electroreduction.

The stability of the electrochemical reactor was further evaluated by operating the system at a predetermined cell potential of 3.8 V, but with catholyte circulating between the cathodic chamber and the reservoir. To monitor performance over time, liquid samples were collected during the experiment and analyzed for formate production. Throughout the entire testing period, the CD remained essentially constant as shown in Figure 6a. The Faradaic charge varied linearly with the time, indicating the involvement charge in the reduction process. This stable current and linear relationship of Faradaic charge with time indicates the sustained activity and effectiveness of the catalyst for formate generation under prolonged operation. In addition to current stability, the Faradaic efficiency (FE) for formate production was examined at various time intervals to assess the selectivity of the electrochemical process (Figure 6b). The results demonstrate that FE values were consistently over 80% over time, suggesting that the reaction pathway favoring formate formation is well maintained during extended electrolysis. The corresponding amounts of formate produced, expressed in millimoles (markers with dotted line in Figure 6b), further confirm steady product formation without noticeable performance degradation. Formate production exhibited a linear increase with time, corresponding to a production rate of about 24 mmol/day over 200 h of continuous operation. We found a huge discrepancy in the rate of production of formate during the long operation without changing the catholyte compared to the experiment where catholyte was changed. As CO_2 is purged into catholyte, potassium hydroxide gets converted first to carbonate and then to bicarbonate, and the pH also keeps decreasing. The addition of formate further decreases the pH, causing poor solubility of CO_2 and increasing mass transportation limitation. This has a direct impact on the CD and the FE. Increasing the pressure of CO_2 can minimize this effect. We speculate that the formate production resumes to the initial rate when fresh potassium hydroxide is used. Overall, these findings highlight the excellent operational stability of

the electrochemical reactor and underscore the robustness of the catalyst at a cell potential of 3.8 V, making it suitable for sustained formate production. The details of the chemistry behind the electrochemical conversion of CO_2 to formate/FA while using aqueous KOH solution can be found in SI.

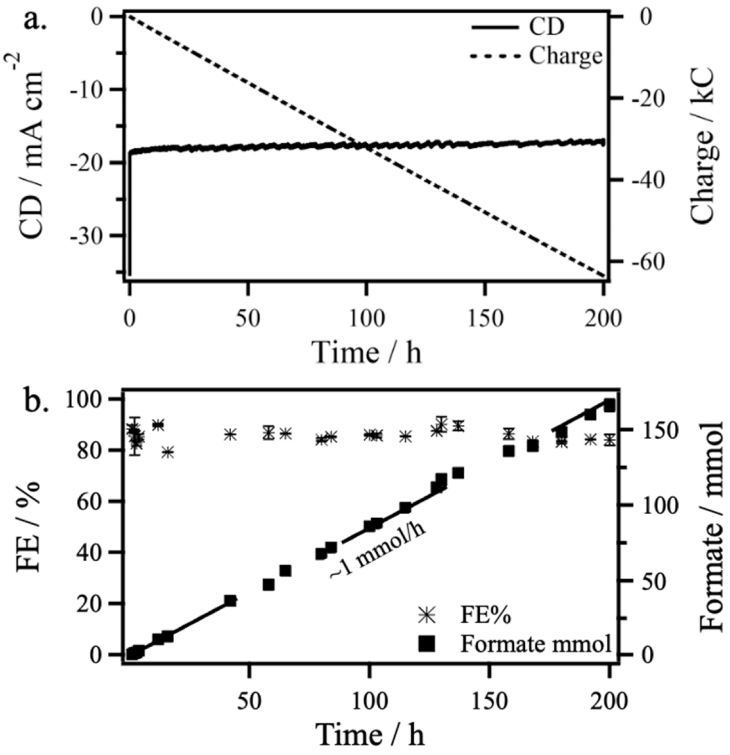

Figure 6. (**a**) Chronoamperometric/chronocoulometric spectra measured at 3.8 V for 200 h. The CD was constant throughout the experiment and the amount of charge passed varied linearly with time. (**b**) The FE and amount of formate produced over 200 h of continuous testing.

4. Technical and Economic Analysis

A high-level techno-economic analysis (TEA) was performed using experimental data to evaluate feasibility of the Cu-modified tin oxide electrocatalyst system to reduce GHG emissions from point sources [56]. The key evaluation parameters included a comprehensive assessment of a detailed accounting of capital costs, a detailed accounting of operation and maintenance costs, an estimated required selling price of the primary product relative to existing markets (no co-products were observed) including assessment of all revenue streams, the assumed unit costs, and current and projected market size and value, as well as the estimated amount of CO_2 utilized. The assessment also examined the scalability of the engineered catalyst for commercial-scale production and evaluated the capital costs associated with constructing a full-scale electrochemical cell. Engineering estimates, derived from experimental data, were used to determine the required dimensions and specifications of major equipment, including equipment types, construction materials, and anticipated energy consumption. The TEA was structured around five primary components: (1) an overview of the process and the design basis for a representative commercial-scale production facility; (2) development of a block flow diagram (Figure 7), stream tables, equipment list, and a summary of electrical power requirements to establish the basis for the economic evaluation and its key outputs; (3) specification and sizing of major equipment based on stream table data; (4) estimation of capital and operating costs, including identification of the major cost contributors; and (5) process economics and cost per tonne of formate (in the intermediate form of potassium formate).

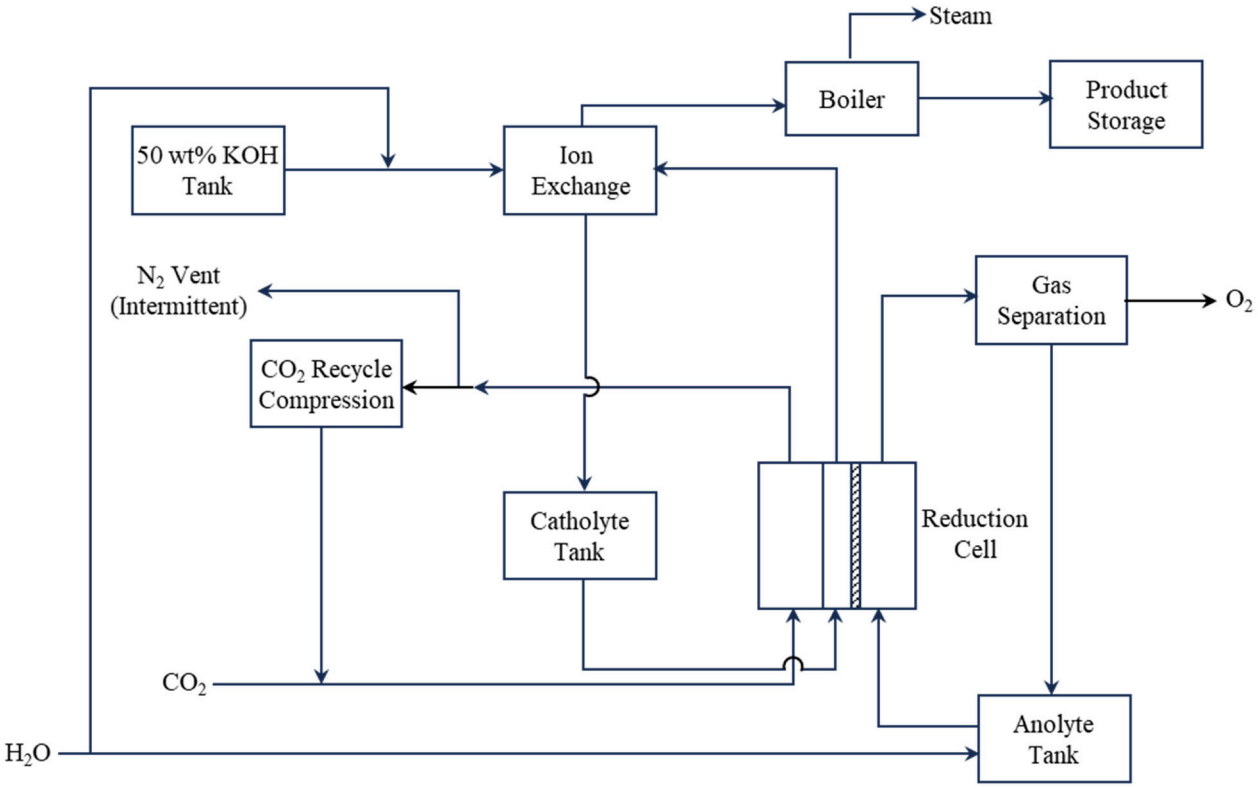

Figure 7. Block flow diagram for synergetic bimetallic electrocatalyst system.

The design basis incorporated the technical process inputs and economic inputs, as well as the system boundaries. The scope of the TEA contain was limited to the conversion of a pure CO_2 stream into aqueous formate. The proposed facility was designed for an annual production capacity of 2000 tonnes of pure formate, operating at an 85% capacity factor. This formate production corresponds to a ~4000 tonnes/yr product stream of 50 wt% concentration potassium formate in water. For the economic assessment, production costs were evaluated based on the 50 wt% potassium formate solution rather than pure formate, reflecting its primary commercial application as a deicing fluid. Purchased equipment costs were estimated for a facility producing 2000 tonnes of pure formate annually, equivalent to 4000 tonnes per year of the 50 wt% potassium formate solution. All costs are provided in November 2022 in US dollars. The economic evaluation of this process uses scaling factors to estimated purchased equipment costs from common engineering modeling programs to develop a purchased equipment cost and a total plant cost estimate. An engineering cost estimator was used for basic components where a reference scaling cost is not readily available. The sizing and costing approaches for key equipment such as the reduction cell and ion exchange unit are derived from the experimental data. Likewise, other large components including liquid pumps, gas/liquid separators, and the anolyte/catholyte tanks are derived from experimental data combined with the engineering cost estimator.

The main components of the process within the context of the TEA include the anode and catalyst-coated cathode within the electrochemical reactor, the anolyte and catholyte tanks and pumps, and ion exchange (IEX) vessels to isolate the produced formate from the catholyte stream as potassium formate. In this configuration, additional IEX treatments can be used to further convert the formate into purified formic acid if desired, although the additional acidification steps are not part of this TEA. The estimated production cost of the 50 wt% potassium formate solution was determined by considering the capital investment, variable operating expenses, and maintenance costs associated with the process technology (Table 1). Variable operating costs constituted the largest portion, accounting for

approximately 70% of the total production cost. This was primarily driven by the electricity consumption of the catalytic electrolyzer, followed by the expense associated with the 50 wt% KOH feed required for regeneration of the ion-exchange (IEX) separation resin.

Table 1. Formate production price calculation from high level TEA.

Tonnes per year of 50 wt% formate produced	3400
Capacity factor	0.85
Amortized Capex per tonne	$307
Operating cost per tonne	$694
50 wt% formate Capex and variable Opex production price $/tonne	$1001

5. Conclusions

Bimetallic electrocatalysts show promise in enhancing activity and selectivity compared to their monometallic counterparts by tuning structure, morphology, and composition. The electrochemical conversion of CO_2 using Cu-doped tin oxide exhibited very high selectivity for formate. The FE for formate was found to be dependent on the cell potential applied for the electrolytes and the membrane selected for the study. Maximum FE of 94% was achieved at the cell potential 3.8 V, which remained above 80% during the 200 h continuous run. The production of formate was also consistent with the FE observed. A high-level TEA was performed using experimental data to assess the economic feasibility of the electrocatalyst system for converting CO_2 captured from point-source emissions into formate. The TEA analysis indicates that variable operating expenses are the dominant contributor to the overall production cost, accounting for approximately 70% of the total. This is primarily attributed to the electrical requirements of operating the catalytic electrolyzer within the overall process, followed by the cost of the 50 wt% KOH feed used for regeneration of the ion exchange (IEX) separation resin. The production price calculated here is very similar to the commercial price as per the data from 2022. This electrochemical system of reduction of CO_2 to formate can be coupled with CO_2 absorption unit where the mass transfer limitation of CO_2 is minimized. This not only reduces notorious greenhouse CO_2 from air but also generates value-added chemicals.

Supplementary Materials: The following supporting information can be downloaded at: https://www.mdpi.com/article/10.3390/electrochem7040039/s1, Figure S1. The variation of pH of aqueous KOH solutions of varied concentrations ranging from 0.1 to 1 M when CO_2 gas is purged continuously. Figure S2. The variation of pH of aqueous $KHCO_3$ solutions of varied concentrations ranging from 0.1 to 1 M when CO_2 gas is purged continuously.

Author Contributions: P.L.K.: writing, investigation, visualization, formal analysis; M.K.G.: catalyst synthesis; M.A.H. and K.A.: investigation, formal analysis; A.O.O.: funding acquisition, conceptualization, visualization, supervision, review, editing, validation; J.T.: funding acquisition, conceptualization, supervision, review, editing, project administration, resources. All authors have read and agreed to the published version of the manuscript.

Funding: This research was funded by Department of Energy under Award, grant number [DE-FE0031920].

Institutional Review Board Statement: Not applicable.

Informed Consent Statement: Not applicable.

Data Availability Statement: The original contributions presented in this study are included in the article/Supplementary Materials. Further inquiries can be directed to the corresponding authors.

Acknowledgments: The authors would like to thank Trimeric Corporation (Buda, TX, USA) for assistance in conducting the technoeconomic analysis.

Conflicts of Interest: The authors declare no conflicts of interest.

Abbreviations

BPM	bipolar membrane
CCE	catalyst-coated electrode
CD	current density
CX	carbon xerogel
FA	formic acid
FE	faradaic efficiency
GDE	gas diffusion electrode
GHG	greenhouse gas
HER	hydrogen evolution reaction
IEX	ion exchange
TEA	techno-economic analysis

References

1. Matin, N.S.; Moreno, D.A.; Abad, K.; Omosebi, A.; Liu, K.; Thompson, J. Life Cycle Assessment of Charge Carrier Mediated Electrocatalytic Reduction of Carbon Dioxide to Formic Acid. *J. Environ. Chem. Eng.* **2025**, *13*, 115184. [CrossRef]
2. Philips, M.F.; Gruter, G.-J.M.; Koper, M.T.; Schouten, K.J.P. Optimizing the Electrochemical Reduction of CO_2 to Formate: A State-of-the-Art Analysis. *ACS Sustain. Chem. Eng.* **2020**, *8*, 15430–15444. [CrossRef]
3. Proietto, F.; Patel, U.; Galia, A.; Scialdone, O. Electrochemical Conversion of CO_2 to Formic Acid Using a Sn Based Electrode: A Critical Review on the State-of-the-art Technologies and Their Potential. *Electrochim. Acta* **2021**, *389*, 138753. [CrossRef]
4. Ma, Z.; Legrand, U.; Pahija, E.; Tavares, J.R.; Boffito, D.C. From CO_2 to Formic Acid Fuel Cells. *Ind. Eng. Chem. Res.* **2020**, *60*, 803–815. [CrossRef]
5. Dey, G.; Fayaz, A.; Muthu, A.P.; Sampath, S. Electrochemical Reduction of CO_2 Using a Metal-Free Polymer Catalyst: Synergy of Pyrrole and Quinone Interfacial Sites. *ACS Appl. Mater. Interfaces* **2026**, *18*, 50821–50832. [CrossRef] [PubMed]
6. Zhang, C.; Liu, T.; Hong, Y.; Zhang, Y.; Yu, Q. Synergistic N and F Co-doping in Carbon Nanotubes for Efficient Metal-Free CO_2 Electroreduction. *Appl. Surf. Sci.* **2026**, *751*, 168151. [CrossRef]
7. Liu, M.; Rao, F.; He, C.; Xu, T.; Liu, C. Theoretical Design of Cage-Like Borophene Single Atom Catalyst for High Efficiency CO2RR. *ACS Sustain. Chem. Eng.* **2025**, *13*, 8103–8115. [CrossRef]
8. Agarwal, A.S.; Zhai, Y.; Hill, D.; Sridhar, N. The Electrochemical Reduction of Carbon Dioxide to Formate/Formic acid: Engineering and Economic Feasibility. *ChemSusChem* **2011**, *4*, 1301–1310. Correction in *ChemSusChem* **2011**, *4*, 1705. https://doi.org/10.1002/cssc.201100220. [CrossRef] [PubMed]
9. Chen, Y.; Kanan, M.W. Tin Oxide Dependence of the CO_2 Reduction Efficiency on Tin Electrodes and Enhanced Activity for Tin/Tin Oxide Thin-Film Catalysts. *J. Am. Chem. Soc.* **2012**, *134*, 1986–1989. [CrossRef] [PubMed]
10. Zhao, S.; Li, S.; Guo, T.; Zhang, S.; Wang, J.; Wu, Y.; Chen, Y. Advances in Sn-based Catalysts for Electrochemical CO_2 Reduction. *Nano-Micro Lett.* **2019**, *11*, 62. [CrossRef] [PubMed]
11. Deng, P.; Wang, H.; Qi, R.; Zhu, J.; Chen, S.; Yang, F.; Zhou, L.; Qi, K.; Liu, H.; Xia, B.Y. Bismuth Oxides with Enhanced Bismuth–Oxygen Structure for Efficient Electrochemical Reduction of Carbon Dioxide to Formate. *ACS Catal.* **2019**, *10*, 743–750. [CrossRef]
12. Zhang, Y.; Li, Z.; Jang, H.; Wei, X.; Qin, Q.; Liu, X. Electrochemical Conversion of CO_2 into $HCOO^-$ in a Synergistic Manner by a Nanocomposite of Zn_2SnO_4/ZnO. *Inorg. Chem. Front.* **2023**, *10*, 1818–1825. [CrossRef]
13. Lee, J.; Liu, H.; Chen, Y.; Li, W. Bismuth Nanosheets Derived by In Situ Morphology Transformation of Bismuth Oxides for Selective Electrochemical CO_2 Reduction to Formate. *ACS Appl. Mater. Interfaces* **2022**, *14*, 14210–14217. [CrossRef] [PubMed]
14. Jiang, X.; Lin, L.; Rong, Y.; Li, R.; Jiang, Q.; Yang, Y.; Gao, D. Boosting CO_2 Electroreduction to Formate via Bismuth Oxide Clusters. *Nano Res.* **2023**, *16*, 12050–12057. [CrossRef]
15. Kim, S.; Dong, W.J.; Gim, S.; Sohn, W.; Park, J.Y.; Yoo, C.J.; Jang, H.W.; Lee, J.-L. Shape-Controlled Bismuth Nanoflakes as Highly Selective Catalysts for Electrochemical Carbon Dioxide Reduction to Formate. *Nano Energy* **2017**, *39*, 44–52. [CrossRef]
16. Bhalothia, D.; Liu, H.-Y.; Chen, S.-H.; Tseng, Y.-T.; Li, W.; Dai, S.; Wang, K.-W.; Chen, T.-Y. The Sub-Nanometer In_2O Clusters on Ag Nanoparticles with Highly Selective Electrochemical CO_2 Reduction to Formate. *Chem. Eng. J.* **2024**, *481*, 148295. [CrossRef]
17. Lv, H.; Guo, F.; Li, J.; Ding, C.; Bi, Z.; Zhang, X.; Zhang, Y.; Chen, B.; Guo, X.; Yu, G. Reverse Reaction Pathways for Efficient CO_2–to–Formic Acid Conversion at Cu_2O–Bi_2O_3 Interfaces in Ionic Liquids. *ACS Catal.* **2026**, *16*, 7633–7645. [CrossRef]

18. Choudhary, H.; Kandwal, A.; Bellamkonda, S.; Dhiman, M. A Review of the Evolving Landscape of Sn-Based Electrocatalysts for CO2 Electroreduction to Formate. *Energy Fuels* **2026**, *40*, 17331–17360. [CrossRef]
19. Chen, S.; Li, W.H.; Jiang, W.; Yang, J.; Zhu, J.; Wang, L.; Ou, H.; Zhuang, Z.; Chen, M.; Sun, X. MOF Encapsulating N-Heterocyclic Carbene-Ligated Copper Single-Atom Site Catalyst Towards Efficient Methane Electrosynthesis. *Angew. Chem. Int. Ed.* **2022**, *61*, e202114450. [CrossRef] [PubMed]
20. Hori, Y. Electrochemical CO_2 Reduction on Metal Electrodes. In *Modern Aspects of Electrochemistry*; Springer: New York, NY, USA, 2008; pp. 89–189. [CrossRef]
21. Pourbaix, M. *Atlas of Electrochemical Equilibria in Aqueous Solutions*, 2nd ed.; NACE International: Houston, TX, USA, 1974.
22. Alvarez-Guerra, M.; Del Castillo, A.; Irabien, A. Continuous Electrochemical Reduction of Carbon Dioxide into Formate Using a Tin Cathode: Comparison with Lead Cathode. *Chem. Eng. Res. Des.* **2014**, *92*, 692–701. [CrossRef]
23. Proietto, F.; Schiavo, B.; Galia, A.; Scialdone, O. Electrochemical Conversion of CO_2 to HCOOH at Tin Cathode in a Pressurized Undivided Filter-Press Cell. *Electrochim. Acta* **2018**, *277*, 30–40. [CrossRef]
24. Del Castillo, A.; Alvarez-Guerra, M.; Solla-Gullón, J.; Sáez, A.; Montiel, V.; Irabien, A. Sn Nanoparticles on Gas Diffusion Electrodes: Synthesis, Characterization and Use for Continuous CO_2 Electroreduction to Formate. *J. CO_2 Util.* **2017**, *18*, 222–228. [CrossRef]
25. Merino-Garcia, I.; Tinat, L.; Albo, J.; Alvarez-Guerra, M.; Irabien, A.; Durupthy, O.; Vivier, V.; Sánchez-Sánchez, C.M. Continuous Electroconversion of CO_2 into Formate Using 2 nm Tin Oxide Nanoparticles. *Appl. Catal. B Environ.* **2021**, *297*, 120447. [CrossRef]
26. Khalil, M.; Aris, A.; Fathurrahman, N.A.; Pratama, Y.; Umar, A.; Hussin, F.; Ivandini, T.A.; Hermawan, A.; Al-Saadi, A.A.; Aroua, M.K. Electrodeposition of Bismuth Nanoclusters Using Deep Eutectic Solvent for Electroreduction of Carbon Dioxide to Formic Acid. *Fuel* **2027**, *428*, 140299. [CrossRef]
27. Lee, W.; Kim, Y.E.; Youn, M.H.; Jeong, S.K.; Park, K.T. Catholyte-Free Electrocatalytic CO_2 Reduction to Formate. *Angew. Chem. Int. Ed.* **2018**, *57*, 6883–6887. [CrossRef] [PubMed]
28. Yang, H.; Kaczur, J.J.; Sajjad, S.D.; Masel, R.I. Electrochemical Conversion of CO_2 to Formic Acid Utilizing Sustainion™ Membranes. *J. CO_2 Util.* **2017**, *20*, 208–217. [CrossRef]
29. Chen, Y.; Vise, A.; Klein, W.E.; Cetinbas, F.C.; Myers, D.J.; Smith, W.A.; Deutsch, T.G.; Neyerlin, K.C. A Robust, Scalable Platform for the Electrochemical Conversion of CO_2 to Formate: Identifying Pathways to Higher Energy Efficiencies. *ACS Energy Lett.* **2020**, *5*, 1825–1833. [CrossRef]
30. Chen, Z.; Zhang, X.; Jiao, M.; Mou, K.; Zhang, X.; Liu, L. Engineering Electronic Structure of Stannous Sulfide by Amino-Functionalized Carbon: Toward Efficient Electrocatalytic Reduction of CO_2 to Formate. *Adv. Energy Mater.* **2020**, *10*, 1903664. [CrossRef]
31. Shen, H.; Jin, H.; Li, H.; Wang, H.; Duan, J.; Jiao, Y.; Qiao, S.-Z. Acidic CO_2-to-HCOOH Electrolysis with Industrial-Level Current on Phase Engineered Tin Sulfide. *Nat. Commun.* **2023**, *14*, 2843. [CrossRef] [PubMed]
32. Jiang, Y.; Shan, J.; Wang, P.; Huang, L.; Zheng, Y.; Qiao, S.-Z. Stabilizing Oxidation State of SnO_2 for Highly Selective CO_2 Electroreduction to Formate at Large Current Densities. *ACS Catal.* **2023**, *13*, 3101–3108. [CrossRef]
33. Ko, Y.-J.; Kim, J.-Y.; Lee, W.H.; Kim, M.G.; Seong, T.-Y.; Park, J.; Jeong, Y.; Min, B.K.; Lee, W.-S.; Lee, D.K. Exploring Dopant Effects in Stannic Oxide Nanoparticles for CO_2 Electroreduction to Formate. *Nat. Commun.* **2022**, *13*, 2205. [CrossRef] [PubMed]
34. Xue, J.; Ji, B.; Zhong, K.; Chen, Y.; Li, X.; Li, J.; Liu, C.; Li, Q.; Zeng, J.; Zheng, T. Promoted CO_2 Electrolysis to Formic Acid Using Single atom Cobalt Alloyed Tin. *Adv. Mater.* **2026**, *38*, e72719. [CrossRef] [PubMed]
35. Duarah, P.; Haldar, D.; Yadav, V.; Purkait, M.K. Progress in the Electrochemical Reduction of CO_2 to Formic Acid: A Review on Current Trends and Future Prospects. *J. Environ. Chem. Eng.* **2021**, *9*, 106394. [CrossRef]
36. Boutin, E.; Robert, M. Molecular Electrochemical Reduction of CO_2 Beyond Two Electrons. *Trends Chem.* **2021**, *3*, 359–372. [CrossRef]
37. Li, J.; Kuang, Y.; Meng, Y.; Tian, X.; Hung, W.-H.; Zhang, X.; Li, A.; Xu, M.; Zhou, W.; Ku, C.-S. Electroreduction of CO_2 to Formate on a Copper-Based Electrocatalyst at High Pressures with High Energy Conversion Efficiency. *J. Am. Chem. Soc.* **2020**, *142*, 7276–7282. [CrossRef] [PubMed]
38. Azenha, C.; Mateos-Pedrero, C.; Lagarteira, T.; Mendes, A.M. Tuning the Selectivity of Cu_2O/ZnO Catalyst for CO_2 Electrochemical Reduction. *J. CO_2 Util.* **2023**, *68*, 102368. [CrossRef]
39. Zheng, T.; Liu, C.; Guo, C.; Zhang, M.; Li, X.; Jiang, Q.; Xue, W.; Li, H.; Li, A.; Pao, C.-W. Copper-Catalysed Exclusive CO_2 to Pure Formic Acid Conversion via Single-Atom Alloying. *Nat. Nanotechnol.* **2021**, *16*, 1386–1393. [CrossRef] [PubMed]
40. Wang, M.; Liu, S.; Chen, B.; Tian, F.; Peng, C. Synergistic Geometric and Electronic Effects in Bi–Cu Bimetallic Catalysts for CO_2 Electroreduction to Formate over a Wide Potential Window. *ACS Sustain. Chem. Eng.* **2022**, *10*, 5693–5701. [CrossRef]
41. Yin, Z.; Gao, D.; Yao, S.; Zhao, B.; Cai, F.; Lin, L.; Tang, P.; Zhai, P.; Wang, G.; Ma, D. Highly Selective Palladium-Copper Bimetallic Electrocatalysts for the Electrochemical Reduction of CO_2 to CO. *Nano Energy* **2016**, *27*, 35–43. [CrossRef]
42. Zhou, H.; You, X.; Huang, Z.; Xu, B.; Shi, Y.; Wang, X.-L.; Yao, Y.-F. Synergistic Dual-Atom Catalysts and Water-Assisted Efficient Electrochemical CO_2 Reduction to Formate. *Chem. Eng. J.* **2025**, *518*, 164299. [CrossRef]

43. Liu, W.; Zhang, Z.; Huo, S.; Ren, Q.; Liu, M. Bimetallic Zn_3Sn_2 Electrocatalyst Derived from Mixed Oxides Enhances Formate Production towards CO_2 Electroreduction Reaction. *Appl. Surf. Sci.* **2023**, *608*, 155110. [CrossRef]
44. Sarfraz, S.; Garcia-Esparza, A.T.; Jedidi, A.; Cavallo, L.; Takanabe, K. Cu–Sn Bimetallic Catalyst for Selective Aqueous Electroreduction of CO_2 to CO. *ACS Catal.* **2016**, *6*, 2842–2851. [CrossRef]
45. Chang, S.; Xuan, Y.; Wang, Q.; Wang, K. Bimetallic In–Sn Core–Shell Catalyst Enabling Highly Efficient Electrocatalytic CO_2 Reduction to Formate. *ACS Appl. Eng. Mater.* **2023**, *1*, 1514–1523. [CrossRef]
46. Bellamkonda, S.; Rasul, S.; Mamlouk, M. Electrochemical CO_2-to-Formate Conversion on Scalable Cu_3Sn Gas Diffusion Electrodes via an OCHO-Mediated Pathway. *ACS Appl. Energy Mater.* **2026**, *9*, 9169–9180. [CrossRef]
47. Eviani, M.; Prakoso, T.; Kusdiana, D.; Widiatmoko, P.; Devianto, H. Stability and Performance of Sn–Zn/C versus Sn–Cu/C Bimetallic Catalysts for Electrochemical Formic Acid Production Under Realistic Diluted Feed Conditions. *ChemElectroChem* **2026**, *13*, e202500435. [CrossRef]
48. Husile, A.; Wang, Z.; Guan, J. Bimetallic Effects in Carbon Dioxide Electroreduction. *Chem. Sci.* **2025**, *16*, 5413–5446. [CrossRef] [PubMed]
49. Yan, Y.; Zhang, Q.; Huang, Y. Progress on Sn-Based Catalysts for Electrochemical Conversion of CO_2 to Formic acid. *J. Earth Environ.* **2026**, *17*, 262–274. [CrossRef]
50. Fang, Z.; Chen, R.; Wang, J.; Imam, A.; Liu, W.; Kokilathasan, N.; Voznyy, O.; Kraatz, H.-B. CuSn Bimetallic Aerogel Supported by B, N Co-doped Graphene Oxide for Selective and Durable Electrochemical Reduction of CO_2 to Formate. *Appl. Catal. A Gen.* **2026**, *725*, 121140. [CrossRef]
51. Li, X.; Deng, N.; Wang, H.; Wen, Q.; Chi, H.; Shui, Y.; Han, J.; Liu, C.; Kang, W. Role Mechanisms, Design Principles and Engineering Strategies of Bimetallic and Multi-Metallic Catalysts for the eCO2RR. *J. Mater. Chem. A* **2026**, *14*, 2644–2688. [CrossRef]
52. Kharel, P.L.; Gnanamani, M.K.; Hoque, M.A.; Abad, K.; Huang, N.; Gao, X.; Liu, K.; Omosebi, A.O.; Thompson, J. Copper-Doped Tin Oxides Supported on Mesoporous Carbon Xerogel for Boosting the Electrochemical Reduction of CO_2 to Formate in Bicarbonate Solution Coupled with CO_2. *Ind. Eng. Che. Res.* **2024**, *63*, 6158–6168. [CrossRef]
53. Hoque, M.A.; Abad, K.; Kharel, P.; Omosebi, A.; Thompson, J. Downstream Separation of Formic Acid with Anion-Exchange Resin from Electrocatalytic Carbon Dioxide (CO_2) Conversion: Adsorption, Kinetics, and Equilibrium Modeling. *Ind. Eng. Chem. Res.* **2024**, *63*, 2779–2790. [CrossRef]
54. Landon, J.; Gao, X.; Kulengowski, B.; Neathery, J.K.; Liu, K. Impact of Pore Size Characteristics on the Electrosorption Capacity of Carbon Xerogel Electrodes for Capacitive Deionization. *J. Electrochem. Soc.* **2012**, *159*, A1861. [CrossRef]
55. Ramdin, M.; Morrison, A.R.; De Groen, M.; Van Haperen, R.; De Kler, R.; Van Den Broeke, L.J.; Trusler, J.M.; De Jong, W.; Vlugt, T.J. High Pressure Electrochemical Reduction of CO_2 to Formic Acid/Formate: A Comparison between Bipolar membranes and Cation exchange Membranes. *Ind. Eng. Chem. Res.* **2019**, *58*, 1834–1847. [CrossRef] [PubMed]
56. Thompson, J. *Intensified Catalytic Conversion of CO_2 into High Value Chemicals*; University of Kentucky: Lexington, KY, USA, 2023.

Disclaimer/Publisher's Note: The statements, opinions and data contained in all publications are solely those of the individual author(s) and contributor(s) and not of MDPI and/or the editor(s). MDPI and/or the editor(s) disclaim responsibility for any injury to people or property resulting from any ideas, methods, instructions or products referred to in the content.